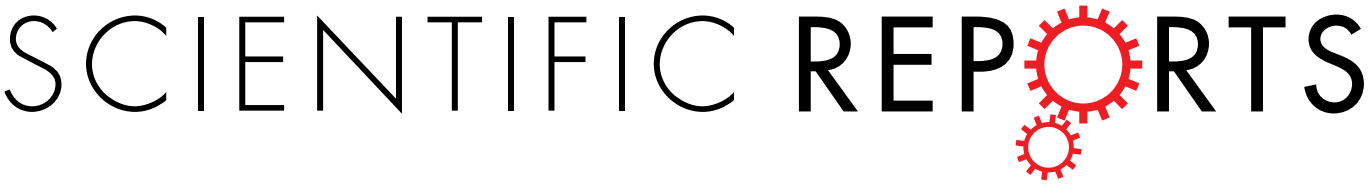

OPEN

A Mathematical Model for Enzyme Clustering in Glucose Metabolism

Miji Jeon[1], Hye-Won Kang[2] & Songon An[1]

Received: 21 September 2017
Accepted: 17 January 2018
Published online: 09 February 2018

We have recently demonstrated that the rate-limiting enzymes in human glucose metabolism organize into cytoplasmic clusters to form a multienzyme complex, the glucosome, in at least three different sizes. Quantitative high-content imaging data support a hypothesis that the glucosome clusters regulate the direction of glucose flux between energy metabolism and building block biosynthesis in a cluster size-dependent manner. However, direct measurement of their functional contributions to cellular metabolism at subcellular levels has remained challenging. In this work, we develop a mathematical model using a system of ordinary differential equations, in which the association of the rate-limiting enzymes into multienzyme complexes is included as an essential element. We then demonstrate that our mathematical model provides a quantitative principle to simulate glucose flux at both subcellular and population levels in human cancer cells. Lastly, we use the model to simulate 2-deoxyglucose-mediated alteration of glucose flux in a population level based on subcellular high-content imaging data. Collectively, we introduce a new mathematical model for human glucose metabolism, which promotes our understanding of functional roles of differently sized multienzyme complexes in both single-cell and population levels.

Glucose metabolism consists of glycolysis and gluconeogenesis. Glycolysis converts glucose into pyruvate, whereas gluconeogenesis reverses the sequential reactions to produce glucose[1]. In normal healthy cells, glucose is converted into pyruvate. Pyruvate then shuttles to mitochondria for oxidative phosphorylation in the presence of oxygen. If the oxygen is limited, however, pyruvate becomes lactate. In addition to its association with energy metabolism, glucose also plays an important role in building block biosynthesis, including the pentose phosphate pathway and serine biosynthesis. This is particularly important in cancer cells because glucose metabolism is dysregulated in proliferating cancer cells in which glucose diverts into building block biosynthesis even in the presence of oxygen. Hence, understanding the mechanism of glucose flux regulation between energy metabolism and building block biosynthesis is important to address altered metabolic phenotypes in human cancer as well as other chronic diseases, including but not limited to diabetes and obesity[2].

Meanwhile, multienzyme metabolic complexes catalyzing glycolysis have been identified in various organisms, including protists, plants, yeast, mammalian neurons and erythrocytes, and human cancer cells[3]. Recently, it has been shown that human liver-type phosphofructokinase 1 (PFKL) forms cytoplasmic clusters in human cancer cells and further colocalizes with other cytoplasmic rate-limiting enzymes of the pathway, including human liver-type fructose-1,6-bisphosphatase (FBPase), pyruvate kinase M2 (PKM2), and phosphoenolpyruvate carboxykinase 1 (PEPCK1), thus indicating the formation of a multienzyme complex, namely the glucosome[4]. The size of glucosome clusters becomes larger in human breast carcinoma cells (Hs578T), relative to non-cancerous human breast tissue cells (Hs578Bst), demonstrating the spatial alteration of glucose metabolism in cancer cells[4]. Similarly, tumor-promoting hypoxic conditions also increased the size of glucosome clusters in human hepatocellular carcinoma cells (HepG2)[5]. Importantly, our quantitative high-content imaging data[4] supported a hypothesis that the glucosome clusters regulate the direction of glucose flux between energy metabolism and building block biosynthesis in a cluster size-dependent manner. Unfortunately, however, it has been challenging to prove the hypothesis experimentally by measuring metabolic activities of various sized glucosome clusters at subcellular levels.

In parallel, several mathematical models for glycolysis have been developed using ordinary differential equations (ODEs) for various model organisms: e.g., bacteria, yeast, virus and human (erythrocytes and liver cells)[6–11]. Along with incorporating *in vitro* kinetic parameters of the enzymes in glycolysis, some ODE-mediated models

[1]Department of Chemistry and Biochemistry, University of Maryland Baltimore County (UMBC), 1000 Hilltop Circle, Baltimore, MD, 21250, USA. [2]Department of Mathematics and Statistics, University of Maryland Baltimore County (UMBC), 1000 Hilltop Circle, Baltimore, MD, 21250, USA. Correspondence and requests for materials should be addressed to H.-W.K. (email: hwkang@umbc.edu) or S.A. (email: san@umbc.edu)

describe the importance of bistable behavior in glycolysis with strong emphasis on the known allosteric regulation of the rate-limiting enzymes[12]. Particularly, recent mathematical models for human liver or cancer cells cover a complicated network beyond glycolysis by including the pentose phosphate pathway, serine biosynthesis, glutamine metabolism, and/or mitochondrial metabolism[13,14]. However, mathematical models for glucose metabolism have barely explained yet how a multienzyme complex influences glucose flux in cancer cells in a cluster size-dependent manner.

In this work, we have constructed a mathematical model to understand how the formation of a multienzyme complex in glucose metabolism affects glucose flux in cancer cells. Since the glucosome is composed of at least four cytoplasmic rate-limiting enzymes of glucose metabolism[4], we have formulated a model to accommodate all the members of the glucosome. Our model indeed reveals the impact of their spatial complexation *in silico* on temporal changes of glycolytic metabolites at a subcellular level in single cells. We further show that our model is capable of predicting metabolic outcomes of a population of cells based on the relative distribution of glucosome clusters in the population. In conclusion, our mathematical model includes not only enzyme kinetics and their allosteric regulation but also spatial compartmentalization of the rate-limiting enzymes of the pathway, thus allowing us to understand the metabolic contributions of glucose flux at both single-cell and population levels.

Model and Methods

A Mathematical Model. We develop a model to investigate how the size of glucosome clusters affects the direction of glucose flux in cancer environment as an indication of the metabolic activity of glucosome clusters in various sizes. Our model involves 7 metabolic intermediates (S_i), 9 enzyme-associated species (E_i) with various forms by which enzyme activities of the rate limiting steps are regulated, 3 metabolic products (P_i), and 28 reactions (Fig. 1 and Tables 1 and 2). Among the fourteen enzymes participating in glycolysis and/or gluconeogenesis, we only focus on the enzyme activities of the glucosome members (i.e., PFKL, FBPase, PKM2, and PEPCK1), which are hypothesized to have different activity levels in a cluster size-dependent manner. In Fig. 1, we present our simplified metabolic pathway with the enzymes involved in the glucosome. All chemical species and reaction rate constants in our pathway are introduced in Tables 1 and 2. An ordinary differential equations (ODE) model was used to describe temporal dynamics of the metabolic network involving enzymatic reactions associated with glucose metabolism. Temporal concentration changes in each metabolic intermediate are determined by propensity functions of the reactions where the intermediate is produced or consumed. Table 3 summarizes the propensity function R_i for the ith reaction. In Table 3, most of the reactions are modeled by the law of mass action, in which the reaction rate is proportional to the substrate concentrations. The allosteric regulations of metabolic enzymes by metabolites are modeled as Michaelis-Menten kinetics, and their propensity functions include rational functions of the substrate concentrations to describe allosteric effects of the corresponding enzymes. Table 4 summarizes a set of all ODEs used in our model.

We also provide reaction rate constants and initial values for the intermediate concentrations used in our model (Tables 1 and 2). We determined the parameters in Tables 1 and 2 using the numerical simulation of the model to be consistent with the qualitative changes in glucose flux in the literature[15]. As shown in Table 1, we assumed that initial concentrations of metabolic intermediates (S_i), products (P_i), PKM2 tetramers (E_3*) and glycosylated PFKL (E_1^{gly}) are at the basal levels and set them as 0.01. We also assumed that no multienzyme complex ($E_{S/M/L}$) is formed at the beginning of simulation. An enzyme concentration of each glucosome member is assumed to be conserved, setting as 100. Assuming that all reaction rate constants for the enzymes are in the same order of magnitude, the reaction rate constants of metabolic enzymes are set to 10 as shown in Table 2. However, we slightly modified the values for k_2, k_{-2}, k_4, and k_{-4} so that glycolysis becomes dominant relative to the metabolic shunt to the pentose phosphate pathway and/or serine biosynthesis in the absence of enzyme clusters (i.e., $P_3 \gg P_1, P_2$). Lastly, we assumed that all the metabolic products are produced ($k_{p/s/f}$) and degraded ($\delta_{p/s/f}$) in the same rates, thus setting them to 5 and 0.5, respectively. Note that we provided both forward and backward reaction rate constants in Table 2, which are separated by comma.

Next, different levels of the enzyme activity depending on the size of glucosome clusters are expressed in terms of the parameters c_i (for medium-sized enzyme clusters) and e_i (for large-sized enzyme clusters) in Table 2. Based on our hypothesis that the medium-sized enzyme clusters promote glucose shunt to the pentose phosphate pathway[4], we decelerated glycolysis (c_2, $c_{-d} \ll 1$) and accelerated gluconeogenesis (c_{-2}, $c_{-6} \gg 1$). Similarly, based on our hypothesis that the large-sized enzyme clusters will shunt glucose flux to serine biosynthesis[4], we changed parameters to direct glucose flux toward serine production (e_2, $e_{-6} \gg 1$, and e_{-2}, $e_{-d} \ll 1$). An enzyme activity in the small-sized clusters is assumed similar to the activity of a freestanding enzyme because the small-sized clusters formed by PFKL do not represent a multienzyme complex[4]. Using the initial values and the reaction rate constants shown in Tables 1 and 2, our mathematical model was simulated using MATLAB to compute temporal changes of glucose flux in different scenarios at the subcellular level. Note that our MATLAB simulation codes are provided in the supplementary document.

Importantly, we have also performed sensitivity analysis of the parameters to investigate how the concentrations of three metabolic products (P_i) are affected by small changes in each parameter that we have incorporated in our model. In the sensitivity analysis, we have used the method of partial rank correlation coefficient (PRCC)[16] to evaluate the level of the linear association between the input values of the parameters and the output concentrations of the metabolic products. To perform the sensitivity analysis, we modified the publically available MATLAB codes which are developed by Kirschner and coworker[16]. The default parameter values were set as the values used in our model, and we defined an interval for each parameter from half of the default value to twice of the default value. Then, we used Latin hypercube sampling[16] to choose each parameter value in the corresponding interval by assuming that each parameter is uniformly distributed in the interval. Afterward, the sampled parameter values were used to calculate the concentrations of the metabolic products at the end time of the simulation.

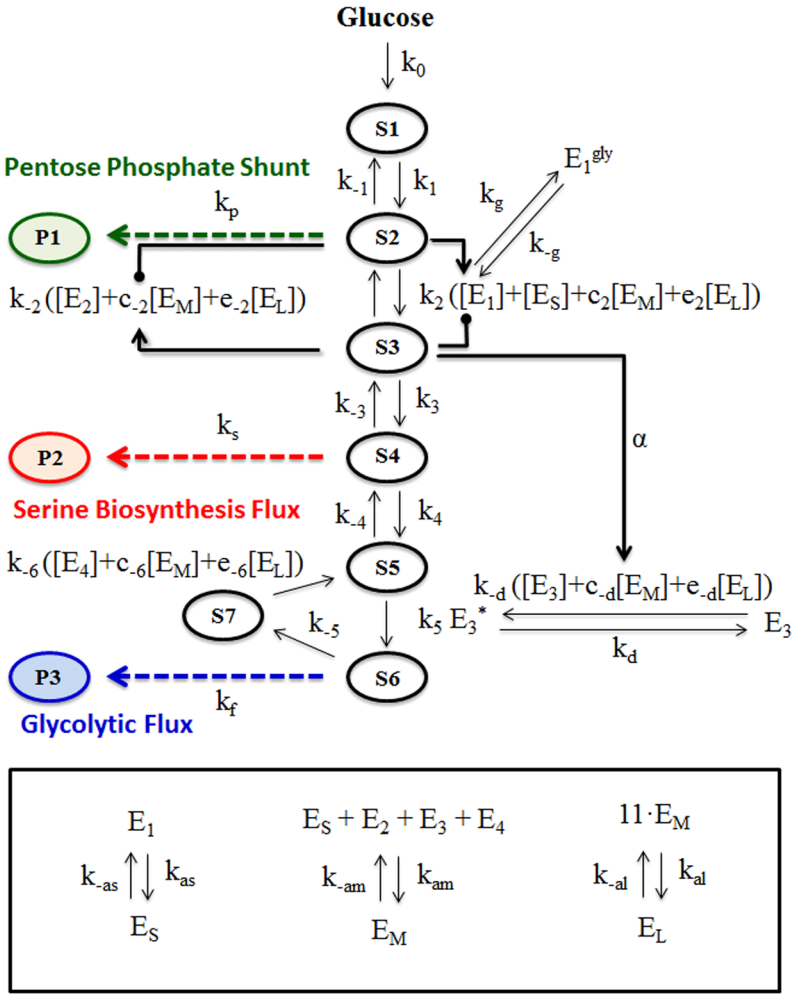

Figure 1. Simplified glucose metabolism with multienzyme complexes. Seven metabolic intermediates are involved in the pathway: S_1 represents glucose, S_2 is fructose-6-phosphate, S_3 is fructose-1,6-bisphosphate, S_4 is 3-phosphoglycerate, S_5 is phosphoenolpyruvate, S_6 is pyruvate, and S_7 is oxaloacetate. Four rate-limiting enzymes are E_1 (phosphofructokinase 1, PFK), E_2 (fructose-1,6-bisphosphatase, FBPase), E_3 (pyruvate kinase M2 dimer, PKM2), and E_4 (phosphoenolpyruvate carboxykinase 1, PEPCK1). Pyruvate kinase M2 catalyzes conversion from S_5 to S_6 when it becomes a tetramer (E_3^*). On the other hand, phosphofructokinase 1 is inactivated after post-translational glycosylation (E_1^{gly}). PFK forms three differently sized clusters: E_S, E_M, and E_L represent small-, medium- and large-sized clusters, where E_M and E_L are multienzyme complexes. To measure the direction of glucose flux, we denote three metabolic products as P_1, P_2, and P_3, which represent metabolic outcomes of the pentose phosphate pathway, serine biosynthesis and the downstream of glycolysis. All the used parameters are summarized in Tables 1 and 2.

We repeated the sampling process described above 20,000 times and calculated the Spearman correlation coefficients, which correspond to PRCCs.

Experimental Methods. *Materials.* The plasmid expressing human PFKL with a monomeric form of enhanced green fluorescent protein (mEGFP) was prepared previously (PFKL-mEGFP)[4]. We have employed PFKL-mEGFP as a marker of the glucosome. 2-Deoxyglucose was purchased from Sigma.

Cell Culture. Human breast carcinoma cells, Hs578T (HTB-126), were obtained from the American Type Culture Collection (ATCC). Hs578T cells were maintained in the Roswell Park Memorial Institute 1640 medium (RPMI1640, Mediatech, Cat# 10-040-CV) supplemented with 10% dialyzed fetal bovine serum (dFBS, Atlanta Biological, Cat# S12850) and 50 μg/mL gentamycin sulfate.

Transfection. To prepare cells for transfection and subsequent imaging, Hs578T cells were gently removed from the culture flask by replacing the culture medium with Trypsin-EDTA solution (Corning, Cat# 25-053-Cl). Fresh, antibiotic-free growth media was subsequently used to harvest and resuspend the cells, followed by plating on glass-bottomed 35 mm Petri dishes (MatTek). When the confluency became ~70–90% on the following day, the cells were transfected with Lipofectamine 2000 (Invitrogen) using the Opti-MEM-I reduced serum media

Variables	Chemical species	Values (non-dimensional)
$S_1(0)$	Glucose	0.01
$S_2(0)$	Fructose-6-Phosphate	0.01
$S_3(0)$	Fructose-1,6-Bisphosphate	0.01
$S_4(0)$	3-Phosphoglycerate	0.01
$S_5(0)$	Phosphoenolpyruvate	0.01
$S_6(0)$	Pyruvate	0.01
$S_7(0)$	Oxaloacetate	0.01
$E_1(0)$	Phosphofructokinase 1	99.99
$E_2(0)$	Fructose-1,6-Bisphosphatase	100
$E_3(0)$	Pyruvate Kinase M2 dimers	99.99
$E_4(0)$	Phosphoenolpyruvate Carboxykinase 1	100
$E_S(0)$	Small-sized enzyme clusters	0
$E_M(0)$	Medium-sized enzyme clusters	0
$E_L(0)$	Large-sized enzyme clusters	0
$E_3^*(0)$	Pyruvate Kinase M2 tetramers	0.01
$E_1^{gly}(0)$	Glycosylated Phosphofructokinase	0.01
$P_1(0)$	Pentose Phosphate Shunt	0.01
$P_2(0)$	Serine Biosynthesis Flux	0.01
$P_3(0)$	Glycolytic Flux	0.01

Table 1. The initial conditions used in the mathematical model for glucose metabolic pathway.

(Opti-MEM-I; Gibco, Cat# 11058). The Opti-MEM-I medium was then exchanged with the fresh antibiotic-free growth medium after a 5 h incubation (37 °C, 5% CO_2, and 95% humidity), followed by ~18–24 h incubation in the CO_2 incubator at 37 °C.

Fluorescence Live-cell Imaging. On the day of imaging (~18–24 h post-transfection), cells were washed with imaging solution (20 mM HEPES (pH 7.4), 135 mM NaCl, 5 mM KCl, 1 mM $MgCl_2$, 1.8 mM $CaCl_2$, and 5.6 mM glucose) for three 10 min incubations, followed by a ~1–2 h incubation at ambient temperature. All samples were then imaged at ambient temperature (~25 °C) with a 60× 1.45 NA objective (Nikon CFI Plan Apo TIRF) using a Photometrics CoolSnap EZ monochrome CCD camera on a Nikon Eclipse Ti inverted C2 confocal microscope. Epifluorescence imaging was carried out using the following filter set from Chroma Technology; mEGFP detection by a set of Z488/10-HC cleanup, HC TIRF Dichroic and 525/50-HC emission filter.

For cell-based high-content imaging assays, 2-deoxyglucose (25 mM) was added to Hs578T cells after washing three times with the imaging solution. Images showing PFKL-mEGFP clusters were acquired before and after cells were incubated with 2-deoxyglucose at various time points (up to 6 hours). Control experiments were also carried out with 167 μL of vehicle (i.e., water). To ensure reproducibility, our experiments were repeated at least five times over the course of a few months. Statistical analysis was performed using two-sample two-tail *t*-tests.

Cluster Size Analysis. Cluster size analysis was accomplished using the *ImageJ* processing software (National Institutes of Health) as we have done before[4]. Briefly, fluorescent wide-field images were processed through *ImageJ* using a custom script and macro that automates the counting of fluorescent clusters using its built-in module, so-called robust automatic threshold selection (RATS). In this analysis, the images were scaled according to the pixel size of the microscope (i.e., 0.12 μm/pixel) before the default parameters for RATS (i.e., noise threshold = 25, λ factor = 3) were used in this analysis. Once fluorescent clusters were selected from an image, the particle analysis module was applied to attain both the number and area of fluorescent clusters within an image. This process was repeated for all subsequent cell images. The operator then evaluated the original cell images against the particle mask to eliminate data in which more than one cluster was counted as a single particle.

Results

Modeling Glucose Metabolism with Multienzyme Complexes. Glucose metabolism consists of glycolysis and gluconeogenesis where three irreversible reactions are involved in glycolysis, four irreversible reactions in gluconeogenesis, and seven reversible reactions in both pathways. In our model, we simplify the 14-step pathway by condensing a few reversible steps into one conversion (Fig. 1). Accordingly, we omit some of the metabolic intermediates such as glucose-6-phosphate, dihydroxyacetone phosphate, glyceraldehyde-3-phosphate, 1,3-bisphosphoglycerate, and 2-phosphoglycerate because they are not directly shuttled to other metabolic pathways. In addition, three metabolic products (P_i) represent three metabolic fates of glycolytic metabolites. Importantly, we focus on four cytoplasmic enzymes which spatially organize into multienzyme clusters (i.e., glucosome clusters)[4]: PFKL, FBPase, PKM2, and PEPCK1. Note that the other ten enzymes are not cytoplasmic or rate-determining in glucose metabolism.

In addition, we incorporated cancer-relevant mechanisms of the four enzymes forming the glucosome. First, pyruvate kinase catalyzes conversion from phosphoenolpyruvate to pyruvate. The M2 isoform of pyruvate kinase

Parameters	Rates	Values (non-dimensional)
k_0	Glucose production	10
k_1, k_{-1}	Conversion to (from) Fructose-6-Phosphate	10, 10
k_2, k_{-2}	Conversion to (from) Fructose-1,6-Bisphosphate	40, 7
k_3, k_{-3}	Conversion to (from) 3-Phophoglycerate	10, 10
k_4, k_{-4}	Conversion to (from) Phosphoenolpyruvate	14, 7
k_5	Conversion to Pyruvate	1
k_{-5}	Conversion to Oxaloacetate	10
k_{-6}	Conversion to Phosphoenolpyruvate from Oxaloacetate	10
k_{as}, k_{-as}	Small enzyme cluster association/disassociation	10, 10
k_{am}, k_{-am}	Medium enzyme cluster association/disassociation	10, 10
k_{al}, k_{-al}	Large enzyme cluster association/disassociation	10, 10
k_g, k_{-g}	Phosphofructokinase glycosylation (de-glycosylation)	1, 1
k_d, k_{-d}	Conversion of Pyruvate Kinase M2 from (to) tetramer to (from) dimer	1, 1
k_p	Pentose Phosphate Shunt	5
k_s	Serine Biosynthesis Shunt	5
k_f	Glycolytic Flux	5
δ_p	Degradation of the Pentose Phosphate Flux	0.5
δ_s	Degradation of Serine Biosynthesis Flux	0.5
δ_f	Degradation of Glycolytic Flux	0.5
c_2	Activation of conversion to Fructose-1,6-Bisphosphate by medium enzyme clusters	0.2
c_{-2}	Activation of conversion from Fructose-1,6-Bisphosphate by medium enzyme clusters	10
c_{-6}	Activation of conversion to Phosphoenolpyruvate from Oxaloacetate by medium enzyme clusters	10
c_{-d}	Activation of conversion from Pyruvate Kinase M2 dimers to Pyruvate Kinase M2 tetramers by medium enzyme clusters	0.1
e_2	Activation of conversion to Fructose-1,6-Bisphosphate by large enzyme clusters	2.5
e_{-2}	Activation of conversion from Fructose-1,6-Bisphosphate by large enzyme clusters	0.1
e_{-6}	Activation of conversion to Phosphoenolpyruvate from Oxaloacetate by large enzyme clusters	10
e_{-d}	Activation of conversion from Pyruvate Kinase M2 dimers to Pyruvate Kinase M2 tetramers by large enzyme clusters	0.05
α	Acceleration of Fructose-1,6-Bisphosphate on Pyruvate Kinase M2 association	1
K_1	Allosteric inhibition by Fructose-1,6-Bisphosphate	1
K_2	Allosteric inhibition by Fructose-6-Phosphate	1
K_3	Allosteric activation by Fructose-1,6-Bisphosphate	1

Table 2. The rate constants used in the mathematical model for glucose metabolic pathway.

(PKM2) is predominantly expressed in cancer cells while suppressing the expression of pyruvate kinase M1 isoform (PKM1)[17]. PKM2 plays an important role in aerobic glycolysis as a dimer by impairing pyruvate production, thus redirecting glucose flux into serine biosynthesis[18,19]. However, a tetrameric form of PKM2 possesses its canonical glycolytic activity in production of pyruvate in cancer cells. We take into account the dimer-tetramer conversion as part of the regulation of glucose metabolism (Fig. 1). Second, PFK catalyzes the conversion of fructose-6-phosphate to fructose-1,6-bisphosphate. Particularly, liver-type PFK (PFKL) is glycosylated in several types of cancer cells under hypoxia conditions, diverting the direction of glucose flux into the pentose phosphate pathway[20]. Our model includes the impact of glycosylation on PFKL as part of the regulation of its metabolic activity in glycolysis. Third, cytoplasmic PEPCK1 plays an essential role in the first step of gluconeogenesis[21]. Recently, a new role of PEPCK1 in tumor cell proliferation was discovered in certain types of cancer cells by controlling carbon metabolic flux through the TCA cycle[22]. However, a molecular level mechanism of PEPCK1 in cancer cells (e.g., post-translational modification-dependent activity or oligomerization-dependent activity) is not firmly established yet to be included in our model. Fourth, FBPase catalyzes the conversion of fructose-1,6-bisphosphate to fructose-6-phosphate. Since FBPase catalyzes the backward reaction of PFK, the activities of PFK and FBPase are reciprocally regulated by various allosteric metabolites. Similarly, an antagonistic role of FBPase for glycolytic flux was validated to play a role in kidney cancer progression[23]. However, other than the well-established allosteric regulation, cancer-specific alteration of FBPase is not established yet to be included in our model.

Unlike many previous mathematical models for glycolysis, we take into account the recent discovery of the glucosome being formed in various sizes in cancer cells. Briefly, various sizes of PFKL clusters in cancer cells are categorized into three subclasses; small, medium and large-sized cluster[4]. Small-sized clusters formed by PFKL are single-enzyme assemblies whereas medium- and large-sized clusters represent spatial organizations of multienzyme complexes. When cancer cells display small-sized clusters, the given cells barely include the other

Reaction	Propensity	Reaction	Propensity	Reaction	Propensity
R_1	k_0	R_{11}	$k_{-5}S_6$	R_{21}	$k_d E_3^*$
R_2	$k_1 S_1$	R_{12}	$k_{-6}(E_4 + c_{-6}E_M + e_{-6}E_L)S_7$	R_{22}	$k_{-d}(E_3 + c_{-d}E_M + e_{-d}E_L)\,(1 + \alpha(S_3)/(S_3 + K_3))$
R_3	$k_{-1}S_2$	R_{13}	$k_{as}E_1$	R_{23}	$k_p S_2$
R_4	$k_2(E_1 + E_S + c_2E_M + e_2E_L)S_2(K_1)/(K_1 + S_3)$	R_{14}	$k_{-as}E_S$	R_{24}	$k_s S_4$
R_5	$k_{-2}(E_2 + c_{-2}E_M + e_{-2}E_L)S_3(K_2)/(K_2 + S_2)$	R_{15}	$k_{am}E_S E_2 E_3 E_4$	R_{25}	$k_f S_6$
R_6	$k_3 S_3$	R_{16}	$k_{-am}E_M$	R_{26}	$\delta_p P_1$
R_7	$k_{-3}S_4$	R_{17}	$k_{al}(E_M)^{11}$	R_{27}	$\delta_s P_2$
R_8	$k_4 S_4$	R_{18}	$k_{-al}E_L$	R_{28}	$\delta_f P_3$
R_9	$k_{-4}S_5$	R_{19}	$k_g E_1$		
R_{10}	$k_5 E_3^* S_5$	R_{20}	$k_{-g}E_1^{gly}$		

Table 3. Propensities of 28 reactions in the glucose metabolic pathway.

Equations

$S = (S_1, S_2, S_3, S_4, S_5, S_6, S_7)^T$, $E = (E_1, E_2, E_3, E_4, E_S, E_M, E_L, E_3^*, E_1^{gly})^T$, $P = (P_1, P_2, P_3)^T$

$\frac{dS}{dt} = \nu_S \mathcal{R}_S(S, E)$, $\frac{dE}{dt} = \nu_E \mathcal{R}_E(S, E)$, $\frac{dP}{dt} = \nu_P \mathcal{R}_P(S, P)$

$\mathcal{R}_S(S, E) = [R_1, R_2, R_3, R_4, R_5, R_6, R_7, R_8, R_9, R_{10}, R_{11}, R_{12}, R_{23}, R_{24}, R_{25}]^T$
$\mathcal{R}_E(S, E) = [R_{13}, R_{14}, R_{15}, R_{16}, R_{17}, R_{18}, R_{19}, R_{20}, R_{21}, R_{22}]^T$
$\mathcal{R}_P(S, P) = [R_{23}, R_{24}, R_{25}, R_{26}, R_{27}, R_{28}]^T$

$$\nu_S = \begin{bmatrix} 1 & -1 & 1 & 0 & 0 & 0 & 0 & 0 & 0 & 0 & 0 & 0 & 0 & 0 & 0 \\ 0 & 1 & -1 & -1 & 1 & 0 & 0 & 0 & 0 & 0 & 0 & -1 & 0 & 0 \\ 0 & 0 & 0 & 1 & -1 & -1 & 1 & 0 & 0 & 0 & 0 & 0 & 0 & 0 & 0 \\ 0 & 0 & 0 & 0 & 0 & 1 & -1 & -1 & 1 & 0 & 0 & 0 & 0 & -1 & 0 \\ 0 & 0 & 0 & 0 & 0 & 0 & 0 & 1 & -1 & -1 & 0 & 1 & 0 & 0 & 0 \\ 0 & 0 & 0 & 0 & 0 & 0 & 0 & 0 & 0 & 1 & -1 & 0 & 0 & 0 & -1 \\ 0 & 0 & 0 & 0 & 0 & 0 & 0 & 0 & 0 & 0 & 1 & -1 & 0 & 0 & 0 \end{bmatrix}$$

$$\nu_E = \begin{bmatrix} -1 & 1 & 0 & 0 & 0 & 0 & -1 & 1 & 0 & 0 \\ 0 & 0 & -1 & 1 & 0 & 0 & 0 & 0 & 0 & 0 \\ 0 & 0 & -1 & 1 & 0 & 0 & 0 & 0 & 1 & -1 \\ 0 & 0 & -1 & 1 & 0 & 0 & 0 & 0 & 0 & 0 \\ 1 & -1 & -1 & 1 & 0 & 0 & 0 & 0 & 0 & 0 \\ 0 & 0 & 1 & -1 & -11 & 11 & 0 & 0 & 0 & 0 \\ 0 & 0 & 0 & 0 & 1 & -1 & 0 & 0 & 0 & 0 \\ 0 & 0 & 0 & 0 & 0 & 0 & 0 & 0 & -1 & 1 \\ 0 & 0 & 0 & 0 & 0 & 0 & 1 & -1 & 0 & 0 \end{bmatrix}$$

$$\nu_P = \begin{bmatrix} 1 & 0 & 0 & -1 & 0 & 0 \\ 0 & 1 & 0 & 0 & -1 & 0 \\ 0 & 0 & 1 & 0 & 0 & -1 \end{bmatrix}$$

Table 4. A system of ODEs for metabolic intermediates, enzymes and their clusters, and metabolic products.

sizes of clusters. However, cancer cells showing medium- and large-sized clusters contain smaller sized clusters. Our cluster size analysis has also revealed that HeLa cells with medium-sized clusters show ~86.1 clusters per cell whereas HeLa cells showing large-sized clusters exhibit ~5.6 large-sized clusters and ~25.1 medium-sized clusters per cell[4]. Accordingly, we assume that 11 medium-sized clusters might form one large cluster in the cytoplasm of cancer cells in our model.

Glucose Flux Analysis at Subcellular Levels. In Fig. 2, metabolic product concentrations are shown in different experimental conditions, which are computed by numerically solving the mathematical model given in Tables 3 and 4. The model results in time-dependent changes of three metabolic products: P_1 represent a metabolic product of the pentose phosphate shunt (green line), P_2 is a metabolic product of serine biosynthesis (red line), and P_3 indicates a metabolic product of the downstream of glycolysis (blue line). In addition, the activity of non-clustering PFKL or clustered PFKL into small sizes are anticipated to be similar in our model. For the simulation of the cases with no cluster or only small-sized PFKL clusters, we set all the parameters related to the formation of medium or large-sized enzyme complexes as zero (i.e., k_{am}, k_{-am}, k_{al}, k_{-al}, c_i, and e_i). Please, note that the parameters for small-sized PFKL clusters (i.e., k_{as} and k_{-as}) were also set to zero when we simulated the case showing no cluster. Consequently, our simulation for no cluster or only small-sized PFKL clusters showed the high level of P_3 relative to those of P_1 and P_2 (Fig. 2A and B), indicating that most of glucose flux flows to glycolysis to produce pyruvate and beyond. However, when the rate-limiting enzymes in glucose metabolism are spatially organized into medium-sized glucosome clusters, the enzymes in medium-sized clusters may have different levels of catalytic activity. Because the increased flux of the pentose phosphate shunt is correlated with the high level of medium-sized clusters in cancer cells[4], our assumption of c_2, $c_{-d} \ll 1$ and c_{-2}, $c_{-6} \gg 1$ resulted in a significant increase of P_1 but decreased the concentrations of P_2 and P_3 (Fig. 2C). In this case, we set the values of k_{al}, k_{-al}, and e_i as zero. Lastly, we considered all the rate-limiting enzymes being assembled into large-sized

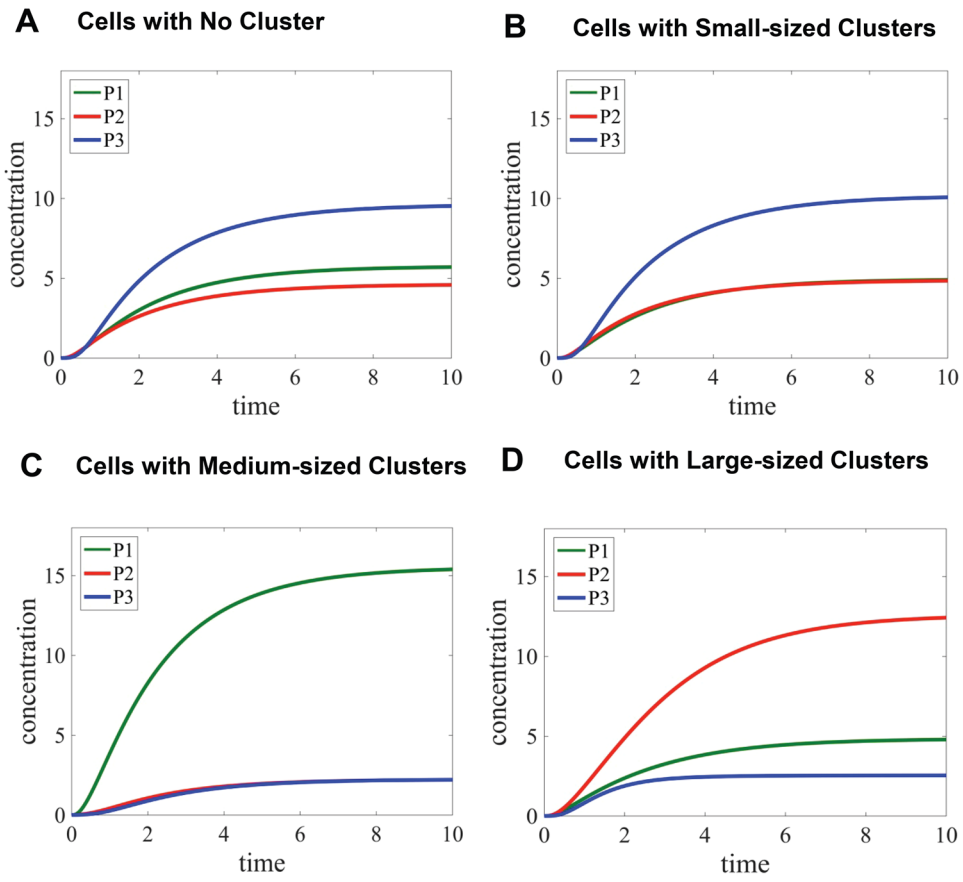

Figure 2. Glucose flux analysis at subcellular levels. Time-dependent changes of metabolic product concentrations (P_1, P_2 and P_3) in single cells are graphed for: (**A**) cells with no spatial organization, (**B**) cells with small-sized PFKL clusters which indicate single enzyme assemblies, (**C**) cells with medium-sized multienzyme complexes, and (**D**) cells with large-sized multienzyme complexes in the presence of smaller clusters. Arbitrary units (a.u.) are used to show relative concentrations or time during our model simulation. P_1, P_2, and P_3 represent metabolic outcomes of the pentose phosphate pathway, serine biosynthesis and the downstream of glycolysis, respectively.

glucosome clusters in the presence of smaller clusters. Because the promotion of large-sized clusters in cancer cells is correlated with the increased flux of serine biosynthesis[4], our assumption of e_2, $e_{-6} \gg 1$ and e_{-2}, $e_{-d} \ll 1$ along with the same assumption of c_i in the previous case resulted in the substantially increased level of P_2 relative to the levels of P_1 and P_3 (Fig. 2D). Collectively, our mathematical model is developed to understand the cluster size-dependent changes of glucose flux in cancer cells.

Sensitivity Analysis. Next, we performed a sensitivity analysis by which we evaluated without bias how the input values of simulation parameters influence the production of specific metabolic flux (P_i). According to the publically available MATLAB codes developed by Kirschner and coworker[16], we modified to calculate PRCCs in our model (Figure S1). If the PRCC values are close to -1 or $+1$, the corresponding parameters have strong correlations with the formation of the given metabolic product. On the other hand, if the correlation coefficient is close to 0, there is no correlation between the input parameters and the given metabolic product. When the absolute values of the PRCCs are greater than ± 0.2 and their p-values are less than 0.01, we defined the corresponding parameters as 'sensitive' parameters (Fig. 3) to determine which simulation parameters are critical for our model and how sensitive each parameter is to understand its contribution to the outcomes of glucose flux. Noticeably, the formation of each metabolic product was sensitive not only to the enzyme activities of the glucosome members but also the efficiencies of enzyme clustering into the certain sizes of glucosomes.

In Fig. 4, we further analyzed a few critical parameters that influence the enzyme activities of the glucosome members (i.e., k_2, k_{-2}, and k_{-d}). Each selected parameter was perturbed in one direction while all other parameter values were fixed as default values as shown in Table 2. The changes in the metabolic product concentrations were then presented under four cases; (i) no spatial organization, (ii) small-sized PFKL clusters, (iii) medium-sized multienzyme complexes, and (iv) large-sized multienzyme complexes. Note that for the cases dealing with the medium-sized or large-sized complexes, the smaller-sized clusters are also formed in the model. When k_2 was decreased from 40 to 10 (Fig. 4A), the conversion from S_2 to S_3 was reduced. We thus observed significant increase in P_1 while decrease in P_2 and P_3. On the other hand, when k_{-2} was increased from 7 to 10 (Fig. 4B), a similar pattern was observed as in Fig. 4A although the changes were small due to the narrow ranges of the parameter.

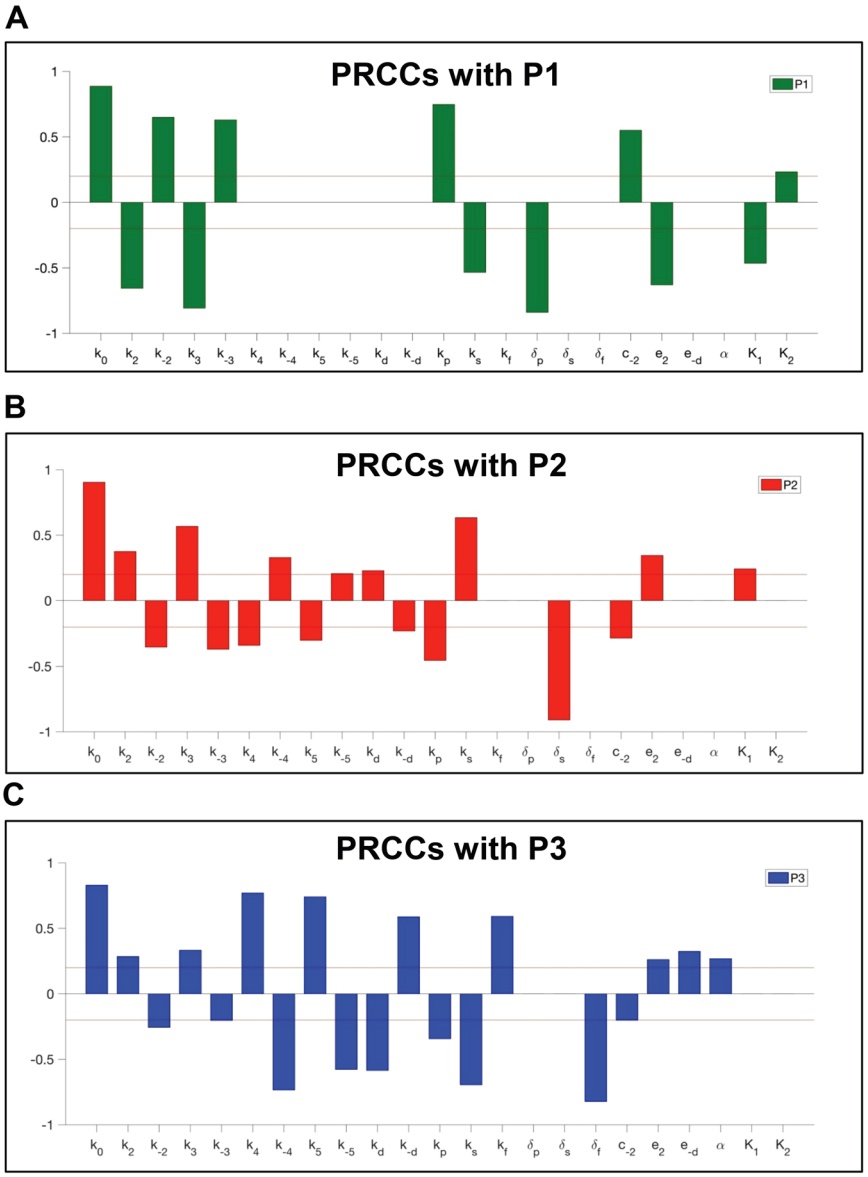

Figure 3. The partial rank correlation coefficients (PRCCs) between the 'essential' input parameters and the concentrations of metabolic products. The PRCCs at *time* = 10 are graphed to provide relative strengths of the correlations between the input parameters and the concentrations of metabolic products (P_1, P_2, and P_3). The horizontal lines at ±0.2 indicate the thresholds we used to distinguish sensitive essential parameters from non-essential parameters. The PRCCs of all parameters are shown in supplementary figure S1. P_1, P_2, and P_3 represent metabolic outcomes of the pentose phosphate pathway, serine biosynthesis and the downstream of glycolysis, respectively.

Finally, when k_{-d} was increased from 1 to 10 (Fig. 4C), glucose flux moved toward the production of P_3, which resulted in significant increase in P_3 and decrease in P_1 or P_2. Note that we did not observe much increase of P_3 in the cases where no spatial organization or only small-sized PFKL clusters are dominant (Fig. 4C) because the flux was already committed toward the production of P_3 in these cases. Collectively, the simulated flux changes reflect the changes of enzymatic activities involved in glucosome clusters.

In Fig. 5, we also analyzed more critical parameters that influence the efficiencies of enzyme clustering into the glucosomes (i.e., c_{-2}, e_2, and e_{-d}). Similarly, each selected parameter was perturbed in one direction while fixing the other parameter values. The changes in the metabolic product concentrations were shown under the four cases as well. When c_{-2} was decreased from 10 to 1 (Fig. 5A), the level of P_1 decreased and that of P_2 increased significantly due to the decreased contribution of the medium-sized cluster to the conversion from S_3 to S_2. When e_2 was decreased from 2.5 to 1 (Fig. 5B), the resulting effect was quite opposite from the one shown Fig. 5A because the decreased e_2 reduces the contribution of the large-sized clusters to the conversion of S_2 to S_3. When e_{-d} was increased from 0.05 to 1 (Fig. 5C), the level of P_2 decreased and that of P_3 increased significantly with

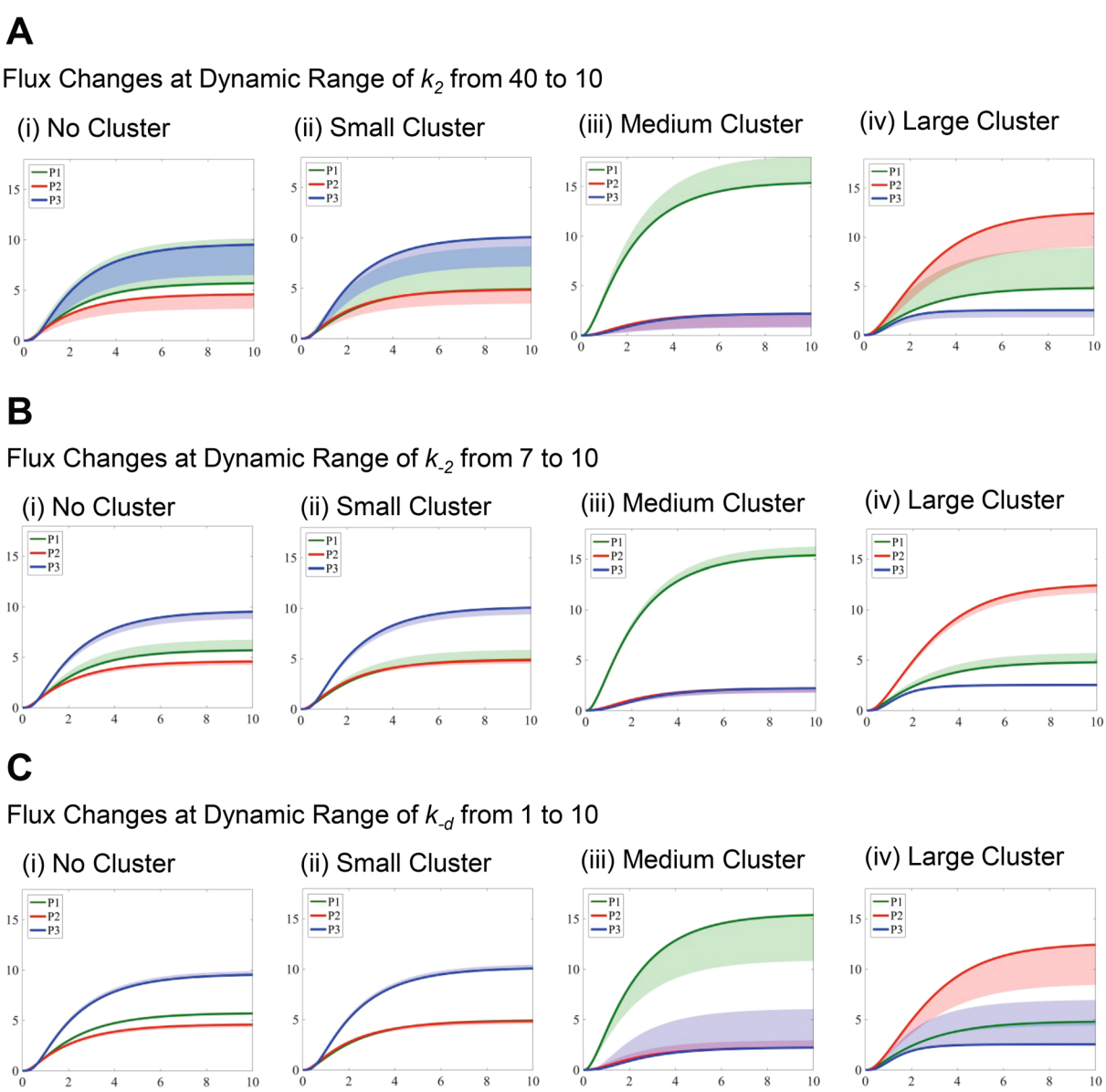

Figure 4. Simulated concentration changes of metabolic products with varying ranges of the catalytic activities of glucosome members. Time-dependent concentration changes of three metabolic products are expressed as shaded regions, when one 'essential' kinetic rate constant is perturbed for k_2 ranging from 40 to 10 (**A**), k_{-2} ranging from 7 to 10 (**B**), and k_{-d} from 1 to 10 (**C**). In each case, time-dependent concentration changes of three metabolic products in single cells are graphed for (i) cells with no spatial organization, (ii) cells with small-sized PFKL clusters, (iii) cells with medium-sized multienzyme complexes, and (iv) cells with large-sized multienzyme complexes.

slight decrease in P_1. This is due to the increased efficiency of the large-sized cluster on its contribution to the conversion of E_3 to E_3^*.

Metabolic Flux Analysis at Ensemble Levels. We have further evaluated our model by quantifying the changes of glucose flux in the presence of methylene blue, fructose-1,6-bisphosphate or epidermal growth factor (EGF), which are known to regulate the direction of glucose flux at ensemble levels[24–29]. As shown in Table 5, we have counted the percentages of cells showing no cluster, small, medium, and large clusters in the absence and presence of the listed glucose flux regulators. In combination with our subcellular flux analysis (Fig. 2), we have computed the time-dependent changes of metabolic products (P_1, P_2, and P_3) at an ensemble level in the four published cases[4]. To predict the levels of metabolic products at an ensemble level, we multiplied the levels of P_1, P_2, and P_3 of the four cases shown in Fig. 2 by the corresponding proportions of the cells showing differently sized clusters. In a control population of Hs578T cells without any exogenous stimulus (Fig. 6A), the level of P_3 appears to be slightly greater than those of P_1 and P_2. However, relative to Fig. 6A, the cancer cells that were treated with methylene blue (Fig. 6B) or fructose-1,6-bisphosphate (Fig. 6C) increase the level of P_1 while decreasing the level

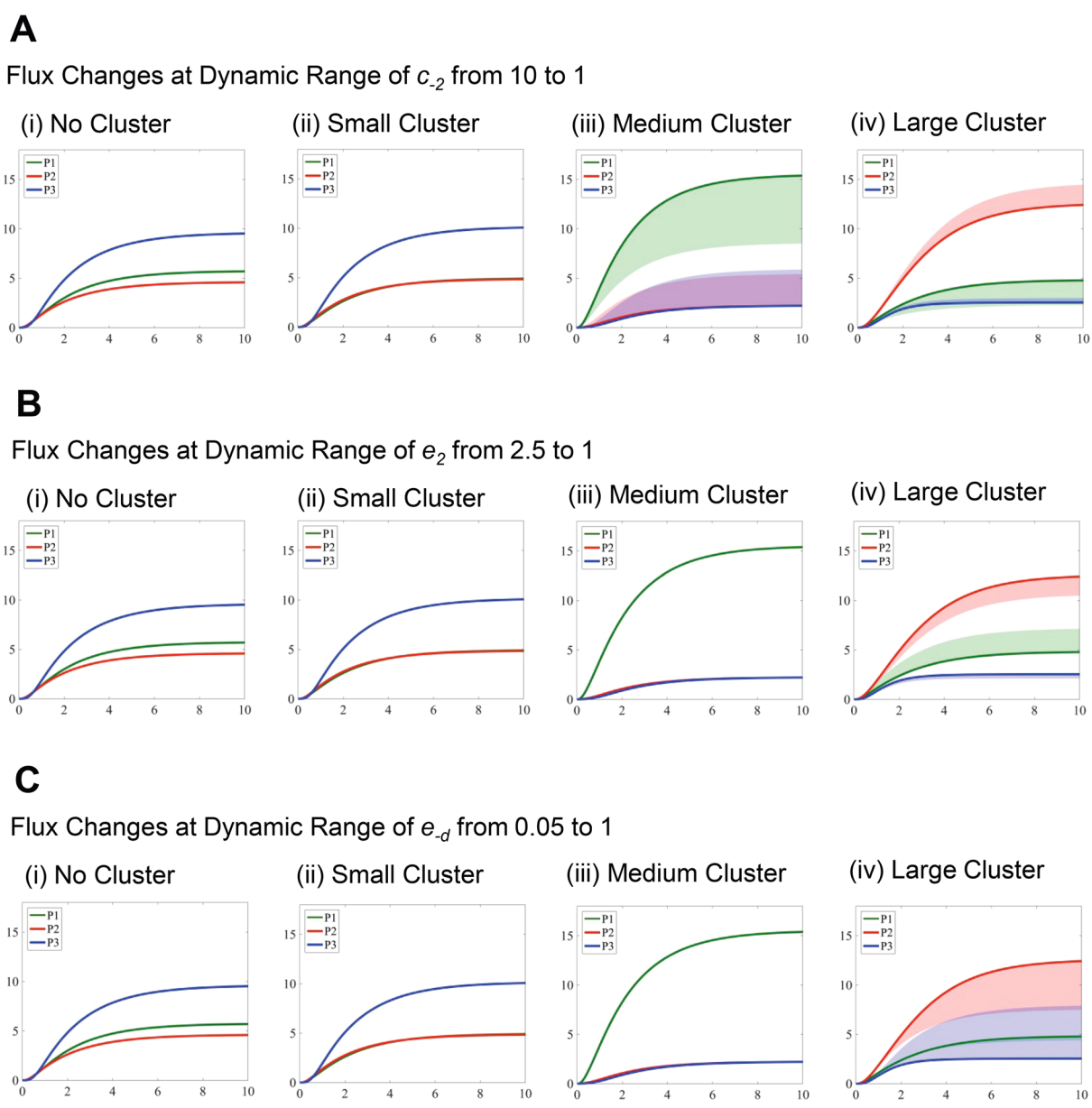

Figure 5. Simulated concentration changes of metabolic products with varying ranges of the clustering efficiency of glucosomes. Time-dependent concentration changes of three metabolic products are expressed as shaded regions, when one 'essential' clustering efficiency is perturbed for c_{-2} ranging from 10 to 1 (**A**), e_2 from 2.5 to 1 (**B**), and e_{-d} from 0.05 to 1 (**C**). In each case, time-dependent concentration changes of three metabolic products in single cells are graphed for (i) cells with no spatial organization, (ii) cells with small-sized PFKL clusters, (iii) cells with medium-sized multienzyme complexes, and (iv) cells with large-sized multienzyme complexes.

of P_3 at an ensemble level. On the other hand, Fig. 6D shows the case where the cancer cells have been treated with EGF. In this case, the level of P_2 increases but the level of P_1 decreases relative to the other cases. It appears clear that the simulation is capable of showing that glucose flux shunt from glycolysis to either the pentose phosphate pathway or the serine biosynthesis at ensemble levels, whose trend is indeed consistent with the already known functions of the glucose flux regulators in populations[24–29]. Collectively, our mathematical model with high-content imaging analysis is adequate to predict metabolic consequences of glucose flux regulators in a population of cancer cells.

Mathematical Prediction of Metabolic Flux with 2-Deoxyglucose at Ensemble Levels. Our model is now applied to assess metabolic consequences of 2-deoxyglucose in Hs578T cells. 2-Deoxyglucose is a competitive inhibitor of phosphoglucose isomerase catalyzing step 2 in glycolysis[30]. However, due to the lack of 2-hydroxyl group, 2-deoxyglucose cannot further metabolize into fructose-6-phosphate in downstream glycolysis, thereby resulting in the inhibition of glycolysis. Accordingly, 2-deoxyglucose appeared to impair cell growth

	No cluster	Small	Medium	Large	Total
Hs578T (Control)	1.6%	58.3%	13.4%	26.7%	100%
Hs578T with Methylene Blue	0.5%	43.0%	25.7%	30.8%	100%
Hs578T with Fructose-1,6-Bisphosphate	0.0%	45.3%	29.1%	25.6%	100%
Hs578T with Epidermal Growth Factor	0.4%	53.1%	7.6%	38.9%	100%
Hs578T with 2-Deoxyglucose	0.0%	34.7%	21.2%	44.1%	100%

Table 5. Ratios of cell distribution showing different-sized clusters in the five environments at the population level.

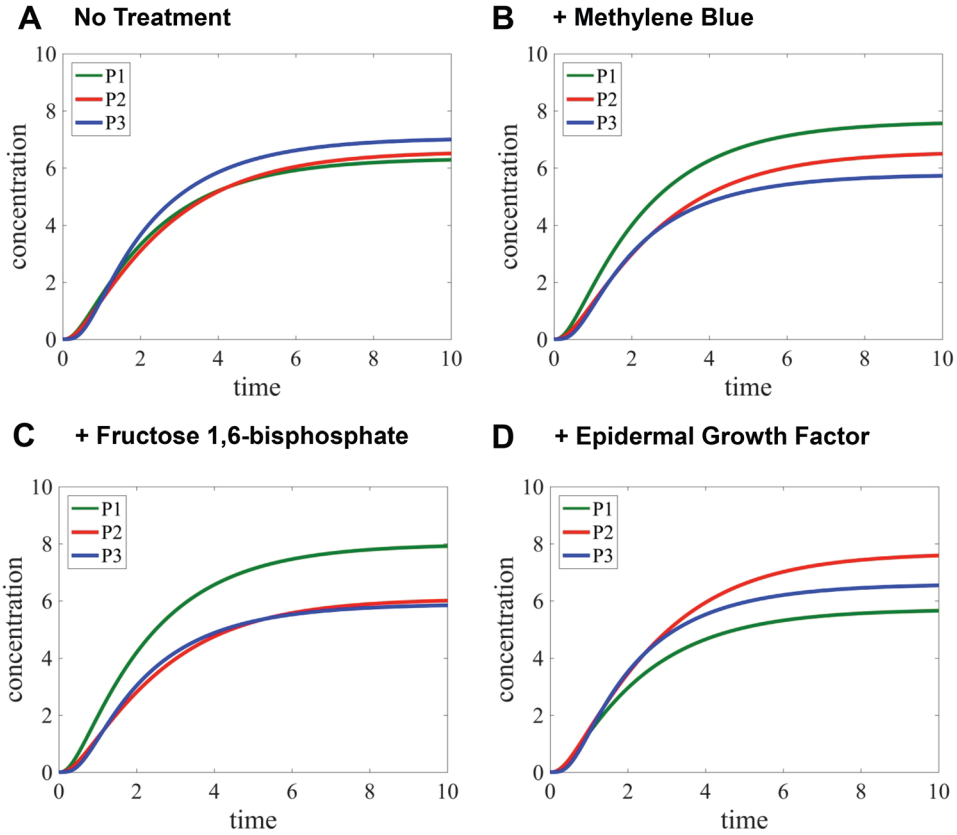

Figure 6. Metabolic flux analysis at ensemble levels. Time-dependent concentration changes of three metabolic products are simulated by our mathematical model in the four scenarios: cancer cells without a glucose flux regulator as a control (**A**), cancer cells that are treated with 5 nM methylene blue (**B**) or 15 mM fructose-1,6-bisphosphate (**C**), and cancer cells with 30 ng/ml epidermal growth factors (**D**). Note that human breast cancer cells (Hs578T) were cultured in the medium of RPMI1640 and 10% dialyzed FBS. P_1, P_2, and P_3 represent metabolic outcomes of the pentose phosphate pathway, serine biosynthesis and the downstream of glycolysis, respectively.

and thus implemented for anti-tumor therapeutics. However, its pharmacological effects on cancer treatment[31–33] remain inconclusive, consequently raising a number of questions particularly including potential metabolic alterations by 2-deoxyglucose in cancer cells.

In this work, we have employed our mathematical model to predict whether 2-deoxyglucose can potentially alter the direction of glucose flux in cancer cells beyond glycolysis inhibition. First, we performed cell-based high-content imaging assays to validate the metabolic effect of 2-deoxyglucose at single cell levels (Fig. 7). Briefly, we expressed PFKL-mEGFP as a glucosome marker in Hs578T cells. To be consistent with Table 5, Hs578T cells were cultured in RPMI1640 with 10% dialyzed FBS. When we treated transfected Hs578T cells with 25 mM of 2-deoxyglucose for 6 hours, the percentage of cells showing small-sized clusters was significantly reduced from 58.3 % to 34.7% (Fig. 7A). Meanwhile, the percentages of cells showing medium- and large-sized clusters were significantly increased from 13.4% to 21.2% and from 26.7% to 44.1%, respectively (Fig. 7A), indicating the strong promotion of glucosome formation and thus metabolic shunts to anabolic pathways.

Subsequently, we computed an ensemble-level outcome of glucose flux in the presence 2-deoxyglucose. Similarly to Fig. 6, we calculated the changes of metabolic outcomes at ensemble levels based on our subcellular

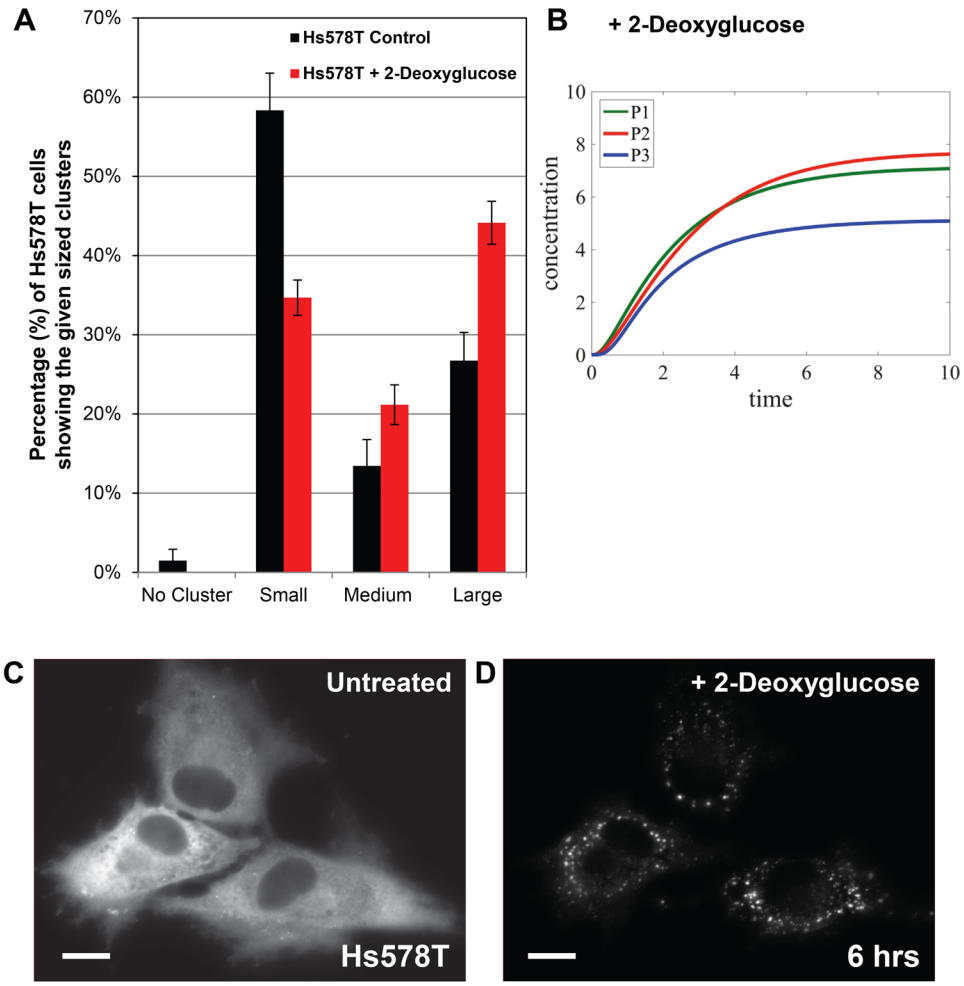

Figure 7. The effect of 2-deoxyglucose on the distribution of Hs578T cells with various sizes of PFKL-mEGFP clusters. The percentage (%) of Hs578T cells displaying each size of PFKL-mEGFP cluster was analyzed in the presence of 2-deoxyglucose. (**A**) The graph shows the average percentages (%) of cells displaying the given sized clusters along with their standard deviations (±) in the absence (black bars) and presence (red bars) of 2-deoxyglucose. At least five independent imaging sessions were performed and total 1200 transfected cells were analyzed. Statistical analyses were performed using two-sample two-tail *t*-tests. $*p < 0.01$. (**B**) Metabolic flux analysis were performed using our mathematical model with the high-content imaging data of 2-deoxyglucose. Relative to a control flux (Fig. 2A), glycolytic flux (P_3) decreased, but the metabolic shunts of glucose to the pentose phosphate pathway (P_1) and serine biosynthesis (P_2) increased. (**C** and **D**) Representative images of Hs578T cells show subcellular localization of PFKL-mEGFP before and after treatment of 2-deoxyglucose (25 mM) for 6 hours. Scale bar, 10 μm.

flux analysis (Fig. 2) and high-content imaging analysis (Fig. 7A, Table 5). Relative to a control flux in Hs578T cells where glycolytic flux reaches to ~7 arbitrary units at $t = 10$ (Fig. 6A), glycolytic flux was indeed inhibited at ~ 5 arbitrary units in the presence of 2-deoxyglucose (Fig. 7B). Importantly, our model provided that metabolic shunts from glycolysis to anabolic biosynthetic pathways were promoted and relatively became dominant in the population of Hs578T cells. Although more experimental validation may be necessary, it is clear that 2-deoxyglucose promoted the formation of glucosome clusters in both single-cell (Fig. 7C,D) and ensemble levels (Fig. 7B). Therefore, we propose that along with the inhibitory role of 2-deoxyglucose in glycolysis, its commitment diverting glucose flux into anabolic pathways may explain in part cancer progression observed during its clinical trials[31].

Discussion

We constructed a simple mathematical model to understand the cluster size-dependent functional contributions of metabolic enzymes and their multienzyme complexes to cancer cell metabolism. Briefly, glycolysis is interconnected with energy metabolism and anabolic biosynthetic pathways, including the pentose phosphate pathway and serine biosynthesis. Three metabolic products (P_i) thus represent downstream pathways of glycolysis, allowing us to investigate how glucose flux changes its direction at metabolic nodes between energy metabolism and anabolic pathways in cancer cells. Based on our experimental data[4], we developed a model to predict that

medium-sized clusters of glucosomes shunt glucose flux into the pentose phosphate pathway whereas large-sized clusters of glucosome divert glucose flux into serine biosynthesis at subcellular levels. Importantly, our model supports that the changes of relative ratios of cancer cells displaying small-, medium- and large-sized clusters in a population appear to be significant enough to influence overall net metabolic outcomes of cancer cells at ensemble levels. Moreover, our mathematical model is further evaluated to predict the effect of 2-deoxyglucose on the fate of glucose, thus providing new quantitative insights of how 2-deoxyglucose alters glucose flux in cancer cells. Collectively, we conclude that our mathematical model supports the hypothesis that glucosomes divert glucose flux into the pentose phosphate pathway and serine biosynthesis in a cluster size-dependent manner.

It is important to emphasize here that our mathematical model accounting for size-dependent metabolic functions of glucosome clusters is significantly different from other models that mostly rely on *in vitro* enzyme kinetics. Our model explains altered glycolysis in cancer cells that redirects glucose flux into the pentose phosphate pathway and serine biosynthesis in a cluster size-dependent manner. Importantly, we can now predict the direction of glucose flux in the presence of small-molecule drug candidates as long as quantitative high-content imaging data is obtained in single-cell levels. Additionally, we can quantify relative partition ratios of glucose flux between glycolysis, the pentose phosphate pathway and serine biosynthesis in various conditions. Collectively, our mathematical model fully integrates various cancer-associated mechanisms discovered in recent years, thus advancing our understanding of cancer cell metabolism in single cells.

References

1. Hers, H. G. & Hue, L. Gluconeogenesis and related aspects of glycolysis. *Annu Rev Biochem* **52**, 617–653 (1983).
2. Scrutton, M. C. & Utter, M. F. Regulation of Glycolysis and Gluconeogenesis in Animal Tissues. *Annu Rev Biochem* **37**, 249 (1968).
3. Schmitt, D. L. & An, S. Spatial Organization of Metabolic Enzyme Complexes in Cells. *Biochemistry* **56**, 3184–3196 (2017).
4. Kohnhorst, C. L. *et al*. Identification of a multienzyme complex for glucose metabolism in living cells. *J Biol Chem* **292**, 9191–9203 (2017).
5. Jin, M. *et al*. Glycolytic Enzymes Coalesce in G Bodies under Hypoxic Stress. *Cell Rep* **20**, 895–908 (2017).
6. Holzhutter, H. G., Jacobasch, G. & Bisdorff, A. Mathematical modelling of metabolic pathways affected by an enzyme deficiency. A mathematical model of glycolysis in normal and pyruvate-kinase-deficient red blood cells. *Eur J Biochem* **149**, 101–111 (1985).
7. Joshi, A. & Palsson, B. O. Metabolic dynamics in the human red cell. *Part I—A comprehensive kinetic model. J Theor Biol* **141**, 515–528 (1989).
8. Munger, J. *et al*. Systems-level metabolic flux profiling identifies fatty acid synthesis as a target for antiviral therapy. *Nat Biotechnol* **26**, 1179–1186 (2008).
9. Rizzi, M., Baltes, M., Theobald, U. & Reuss, M. *In vivo* analysis of metabolic dynamics in Saccharomyces cerevisiae: II. Mathematical model. *Biotechnol Bioeng* **55**, 592–608 (1997).
10. Teusink, B. *et al*. Can yeast glycolysis be understood in terms of *in vitro* kinetics of the constituent enzymes? Testing biochemistry. *Eur J Biochem* **267**, 5313–5329 (2000).
11. Voit, E. O. *et al*. Regulation of glycolysis in Lactococcus lactis: an unfinished systems biological case study. *Syst Biol (Stevenage)* **153**, 286–298 (2006).
12. Mulukutla, B. C., Yongky, A., Daoutidis, P. & Hu, W. S. Bistability in glycolysis pathway as a physiological switch in energy metabolism. *PLoS One* **9**, e98756 (2014).
13. Khazaei, T., McGuigan, A. & Mahadevan, R. Ensemble modeling of cancer metabolism. *Front Physiol* **3**, 135 (2012).
14. Marin-Hernandez, A. *et al*. Modeling cancer glycolysis. *Biochim Biophys Acta* **1807**, 755–767 (2011).
15. Benjamin, D. I., Cravatt, B. F. & Nomura, D. K. Global profiling strategies for mapping dysregulated metabolic pathways in cancer. *Cell Metab* **16**, 565–577 (2012).
16. Marino, S., Hogue, I. B., Ray, C. J. & Kirschner, D. E. A methodology for performing global uncertainty and sensitivity analysis in systems biology. *J Theor Biol* **254**, 178–196 (2008).
17. Mazurek, S., Boschek, C. B., Hugo, F. & Eigenbrodt, E. Pyruvate kinase type M2 and its role in tumor growth and spreading. *Semin Cancer Biol* **15**, 300–308 (2005).
18. Christofk, H. R. *et al*. The M2 splice isoform of pyruvate kinase is important for cancer metabolism and tumour growth. *Nature* **452**, 230–233 (2008).
19. Wong, N., De Melo, J. & Tang, D. PKM2, a Central Point of Regulation in Cancer Metabolism. *Int J Cell Biol* **2013**, 242513 (2013).
20. Yi, W. *et al*. Phosphofructokinase 1 glycosylation regulates cell growth and metabolism. *Science* **337**, 975–980 (2012).
21. Xiong, Y., Lei, Q. Y., Zhao, S. & Guan, K. L. Regulation of Glycolysis and Gluconeogenesis by Acetylation of PKM and PEPCK. *Cold Spring Harb. Symp. Quant. Biol.* **76**, 285–289 (2011).
22. Montal, E. D. *et al*. PEPCK Coordinates the Regulation of Central Carbon Metabolism to Promote Cancer Cell Growth. *Mol Cell* **60**, 571–583 (2015).
23. Li, B. *et al*. Fructose-1,6-bisphosphatase opposes renal carcinoma progression. *Nature* **513**, 251–255 (2014).
24. Bolanos, J. P., Delgado-Esteban, M., Herrero-Mendez, A., Fernandez-Fernandez, S. & Almeida, A. Regulation of glycolysis and pentose-phosphate pathway by nitric oxide: impact on neuronal survival. *Biochim. Biophys. Acta* **1777**, 789–793 (2008).
25. Delgado, T. C., Castro, M. M., Geraldes, C. F. & Jones, J. G. Quantitation of erythrocyte pentose pathway flux with [2-13C]glucose and 1H NMR analysis of the lactate methyl signal. *Magn. Reson. Med.* **51**, 1283–1286 (2004).
26. Kelleher, J. A., Chan, P. H., Chan, T. Y. & Gregory, G. A. Energy metabolism in hypoxic astrocytes: protective mechanism of fructose-1,6-bisphosphate. *Neurochem. Res.* **20**, 785–792 (1995).
27. Lewis, I. A., Campanella, M. E., Markley, J. L. & Low, P. S. Role of band 3 in regulating metabolic flux of red blood cells. *Proc. Natl. Acad. Sci. USA* **106**, 18515–18520 (2009).
28. Martino, G. *et al*. The fate of human peripheral blood lymphocytes after transplantation into SCID mice. *Eur. J. Immunol.* **23**, 1023–1028 (1993).
29. Possemato, R. *et al*. Functional genomics reveal that the serine synthesis pathway is essential in breast cancer. *Nature* **476**, 346–350 (2011).
30. Wick, A. N., Drury, D. R., Nakada, H. I. & Wolfe, J. B. Localization of the primary metabolic block produced by 2-deoxyglucose. *J Biol Chem* **224**, 963–969 (1957).
31. Raez, L. E. *et al*. A phase I dose-escalation trial of 2-deoxy-D-glucose alone or combined with docetaxel in patients with advanced solid tumors. *Cancer Chemother Pharmacol* **71**, 523–530 (2013).
32. Ralser, M. *et al*. A catabolic block does not sufficiently explain how 2-deoxy-D-glucose inhibits cell growth. *Proc Natl Acad Sci USA* **105**, 17807–17811 (2008).
33. Urakami, K., Zangiacomi, V., Yamaguchi, K. & Kusuhara, M. Impact of 2-deoxy-D-glucose on the target metabolome profile of a human endometrial cancer cell line. *Biomed Res* **34**, 221–229 (2013).

Acknowledgements

We would like to thank Dr. Bradford Peercy (UMBC) for critically reading our manuscript. We thank UMBC for providing the Start-Up funds (S.A. and H.-W.K., respectively). This work was also supported in part by the 2016 AACR-Bayer Innovation and Discovery Grant (#16-80-44-ANSO; S.A.), NIH/NIGMS (R01GM125981; S.A.), and the National Science Foundation (DMS-1620403; H.-W.K.). M.J. was also funded in part by NIH/NIGMS Training Grant (T32GM066706).

Author Contributions

S.A. and H.-W.K. designed research and developed a model; M.J. performed high-content imaging experiments; H.-W.K. performed numerical simulation of the models; and S.A. and H.-W.K. wrote the paper.

Additional Information

Supplementary information accompanies this paper at https://doi.org/10.1038/s41598-018-20348-7.

Competing Interests: The authors declare no competing interests.

Publisher's note: Springer Nature remains neutral with regard to jurisdictional claims in published maps and institutional affiliations.

Open Access This article is licensed under a Creative Commons Attribution 4.0 International License, which permits use, sharing, adaptation, distribution and reproduction in any medium or format, as long as you give appropriate credit to the original author(s) and the source, provide a link to the Creative Commons license, and indicate if changes were made. The images or other third party material in this article are included in the article's Creative Commons license, unless indicated otherwise in a credit line to the material. If material is not included in the article's Creative Commons license and your intended use is not permitted by statutory regulation or exceeds the permitted use, you will need to obtain permission directly from the copyright holder. To view a copy of this license, visit http://creativecommons.org/licenses/by/4.0/.

© The Author(s) 2018